EUROFUSION WPMAT-PR(15) 14078

Yu.F. Zhukovskii et al.

Ab initio simulations on migration paths of interstitial oxygen in corundum

Preprint of Paper to be submitted for publication in
Nuclear Instruments and Methods in Physics Research
Section B

This work has been carried out within the framework of the EUROfusion Consortium and has received funding from the Euratom research and training programme 2014-2018 under grant agreement No 633053. The views and opinions expressed herein do not necessarily reflect those of the European Commission.

ELSEVIER

Nuclear Instruments and Methods in Physics Research B

journal homepage: www.elsevier.com

Ab initio simulations on migration paths of interstitial oxygen in corundum

Yuri F Zhukovskii,* Alexander Platonenko, Sergei Piskunov, and Eugene A Kotomin

Institute of Solid State Physics, University of Latvia, 8 Kengaraga, Riga, LV-1063, Latvia

ARTICLE INFO

Article history:
Received
Received in revised form
Accepted
Available online

Keywords:
α-Al_2O_3 (corundum, sapphire)
Oxygen interstitial
Transition states of migration
Hybrid DFT-LCAO calculations

ABSTRACT

Ionizing radiation produces in Al_2O_3 (corundum) crystals primary Frenkel pairs of complementary defects (in oxygen sublattice these are oxygen vacancies and interstitial oxygen ions, V_O-O_i). The interstitial O_i atoms begin to migrate above some temperature and create the dumbbell pairs with regular oxygen atoms (O_{reg}-O_i). We have calculated the optimal dumbbell configurations and optimized further migration paths (*i.e.*, O_i interstitial can break the bond with one O_{reg} atom and moves towards another, one of four next-neighbor O_{reg} atoms). To simulate all possible O_i migration trajectories, we have performed large-scale hybrid DFT-LCAO PBE0 calculations on 2×2×1 supercells of defective α-Al_2O_3 crystals using *CRYSTAL14* computer code. The limiting barrier height for oxygen interstitial 3D migration is estimated as 1.3 eV.

1. Introduction

α-Al_2O_3 (corundum, sapphire) crystals are widely used for numerous industrial applications, such as catalyst support, in solid state lasers and photovoltaic devices.[1] Due to both high radiation resistance and wide band gap (8.8 eV),[2] α-Al_2O_3 is also used as an effective detector of ionizing radiation. Moreover, its potential applications include components of breeder blanket and diagnostic windows, as well as coatings in future fusion reactors, in order to avoid the permeation of light gases.[3,4] Various types of defects created by irradiation of corundum by high-energy neutrons and ions have been previously intensively studied.[5-12] Structural changes as a result of exposure to radiation appears mainly as neutral and charged aluminium and oxygen vacancies (V_{Al} and V_O),[5-7,13,14] interstitial atoms (Al_i and O_i),[5,7,14] complementary Frenkel pairs in two sublattices (V_{Al}+Al_i)[7] and (V_O+O_i).[14] Recently, it has been shown theoretically[14] that O_i in corundum could form the dumbbell configuration with a regular oxygen ions, (O_{reg}+O_i), similar to the MgO crystals[14] and alkali halides (where the dumbbells are called the *H* centers)[16]. This fact could considerably affect the defect migration energy. Note that the formation energies of defects in α-Al_2O_3 were calculated so far using mainly the Density Functional Theory (DFT) within plane-wave formalism.[17]

A number of *ab initio* calculations on anion dumbbells were performed earlier on both alkali metal chlorides (*fcc* NaCl, KCl[16,18,19] and *bcc* CsBr[20] as well as alkaline-earth metal fluorides (CaF_2, MgF_2 and SrF_2)[21-23], where the equilibrium defect configurations, optical properties and possible migration trajectories of interstitial halogen atoms were simulated. Analogous simulation of dumbbells in metal oxides was earlier performed for *fcc*-MgO bulk only, where migration paths of O_i atom were considered along both [111] and [110] crystallographic axes.[15] In the recent study,[14] we have performed *ab initio* calculations on (V_O+O_i) Frenkel pairs and oxygen interstitials in the oxygen sublattice of the α-Al_2O_3. It was shown that the dumbbell (O_{reg}+O_i) is energetically more favourable than the isolated interstitial atom. The dumbbell has the effective charge -1.1 *e,* close that the effective charge for a regular ion O_{reg} in corundum, *i.e.*, the dumbbell is a neutral defect with respect to the perfect lattice.

In this study, we perform hybrid DFT-LCAO calculations, in order to study possible *migration paths* of a neutral radiation-induced O_i atom in corundum along four different trajectories, beginning with the optimized dumbbell configuration in α-Al_2O_3 lattice. We also estimate the activation *migration barriers* along these paths as well as structural relaxations around the interstitial atom trajectories and redistributions of the electronic charges within three coordination spheres around moving O_i ions. Determination of the interstitial migration energy is important for the material stability/resistivity under intensive irradiation and for interpretation of the experimental data on defect accumulation and annealing kinetics.

2. Theoretical background

2.1. Computational details

Defective α-Al_2O_3 crystals containing either Frenkel defect pair (V_O+O_i) or dumbbell (O_{reg}+O_i) have been using method of the crystalline orbitals expanded into linear combination of atomic orbitals (CO LCAO). To perform these calculations, we use the *CRYSTAL14* code,[24] for periodic systems, which employs Gaussian-type functions (GTFs) centered on atomic nuclei as the basis sets (BSs). We have used the all-valence BS for atomic GTFs of oxygen (constructed using pure *s*- and *d*- as well as hybrid *sp*-AOs in the form of 6*s*-2111*sp*-1*d* as described

* Corresponding author. Tel.: +371-288-24-271; fax: +371-671-32-778; e-mail: quantzh@latnet.lv

elsewhere)[25] as well as the effective core pseudopotential (ECP) with $3s^2 3p^1$ external shell developed for aluminum.[26]

To estimate the formation energy of O_i interstitial and its migration barriers in α-Al_2O_3 lattice, the basis set for a free oxygen molecule has been extended by adding *sp*-function with more diffuse exponents. The 3-parameter hybrid exchange-correlation DFT-LCAO functional suggested by Becke (PBE0)[27] has been used. To provide a balanced summation in both direct and reciprocal lattices, the reciprocal space integration has been performed by sampling the Brillouin zone with the 4×4×4 Pack-Monkhorst mesh.[28] Calculations are considered as converged only when the total energy differs by less than 10^{-7} a.u. in two successive cycles of the self-consistency procedure. All the calculations have been performed with total geometry optimization avoiding any symmetry restrictions except *P*1. When modeling the point defects in corundum bulk, the 2×2×1 and 3×3×1 supercell models containing 120 and 270 atoms, respectively, have been adopted. Within the SCF procedure, the accuracies (tolerances) 10^{-7}, 10^{-7}, 10^{-7}, 10^{-7}, 10^{-14} have been chosen for calculations of Coulomb and exchange integrals.[24] The effective charges on atoms have been estimated using Mulliken population analysis.[29]

The formation energies for interstitial O_i atom in different positions in the lattice (including (O_{reg}+O_i) dumbbell), V_O vacancy and Frenkel pair (V_O+O_i) presented in Table 1 have been calculated from the relevant total energies using the equations:

$$E_{form}^{O_i} = E_{tot}^{O_i} - E_{tot}^{Al_2O_3\,(perfect)} - E_{tot}^{\frac{1}{2}O_2}, \qquad (1)$$

$$E_{form}^{V_O} = E_{tot}^{V_O} - E_{tot}^{Al_2O_3\,(perfect)} + E_{tot}^{\frac{1}{2}O_2}, \qquad (2)$$

$$E_{form}^{Frenkel\ pair} = E_{tot}^{Frenkel\ pair} - E_{tot}^{Al_2O_3\,(perfect)}. \qquad (3)$$

2.2. Atomistic model for migration paths of O_i atom in α-Al_2O_3

In our previous paper,[8] we have calculated the (V_O+O_i) Frenkel pair and interstitial oxygens using 2×2×1 supercells.

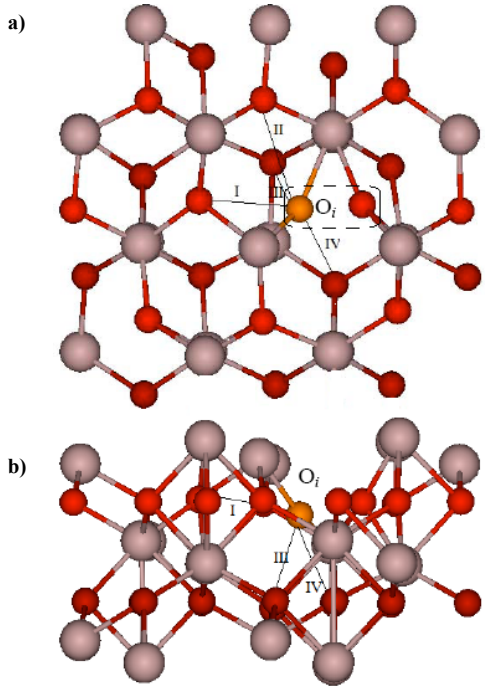

Figure 1. Atop (0001) (a) and aside (b) views of four migration paths I-IV for O_i atom (shown as orange ball) in α-Al_2O_3 lattice. Small and large balls correspond to O and Al atoms, respectively. Dumbbell (O_i-O_{reg}) pair is shown by a dotted rectangle.

Calculations on all the defective α-Al_2O_3 structures have been performed with the defect structure optimization based on the total energy minimization.[24] The energies of the transition states (O_i migration barriers) have been obtained using the distinguished reaction coordinate technique following the method[30] as implemented in the *CRYSTAL14* code. The optimized migration pattoh corresponds to a trajectory of local minimum points on the potential energy surface (PES). Usually, the optimized structure is found using a "minimization" algorithm which may turn out to be either local minima or transition state (TS) structures. For a comparison with these results[14] we have performed here additional calculations on a larger, 3×3×1 supercell of α-Al_2O_3 containing anion point and pairwise defects, including formation energies and effective charges.

3. Stability of (O_{reg}+O_i) dumbbell and mobility of O_i atoms

3.1. Calculated formation energy and charges for O_i and V_O

According to the results obtained in calculations for both 2×2×1 and 3×3×1 supercells of defective corundum, oxygen atoms (O_i) kicked off from the regular sites by irradiation, prefer to form the dumbbells with O_{reg} atoms, rather than to occupy centers of octahedral interstitials (the dumbbell formation occurs with the energy gain of 3.88 eV, as follows from Table 1). An additional electron density (-0.5 *e*) is attracted to O_i from surrounding lattice ions, mostly nearest O_{reg}, *i.e.*, a strong charge redistribution occurs between O_{reg} and O_i towards creation of quasi-molecule O_{reg}+O_i.

Table 1. Defect formation energies, Eqs. (1-3), the atomic effective charges and the bond length of (O_{reg}+O_i) dumbbell

Supercell	Formation energy, eV				$d_{O\text{-}O}$[b], Å	Effective charge, *e*		
	O_i atom in:		V_O vacancy	Frenkel pair[d]		O_{reg}+O_i	O_{reg}[c]	O_i
	center[a]	dumbbell						
2×2×1	8.03	4.21	7.60	11.81	1.404	- 1.102	-0.603	-0.499
3×3×1	8.03	4.22	7.61	11.80	1.404	-1.104	-0.605	-0.499

[a]position in the center of interstitial octahedron between six O_{reg} atoms;
[b]equilibrium distance between O_{reg} and O_i atoms in dumbbell pair (the corresponding distance in a neutral O_2 molecule is 1.21 Å,[31] whereas 1.4 Å is equilibrium one in peroxy radical O_2^{2-});
[c]the effective charge of O_{reg} atom in perfect corundum is -1.0 *e*, due to contribution from partially covalent Al-O bonds,[14] while a fraction of this charge moves to oncoming O_i during the dumbbell formation;
[d]optimized distance in Frenkel pair is estimated 4.4[14] and 5.5 Å, respectively.

Obviously, the difference in results between 2×2×1 and 3×3×1 supercells is very small which allows us to concentrate efforts on the simulation of O_i atom migration within computationally much less expensive 2×2×1 model. It is also clear that migration of O_i atom can occur *via* creation of chain between newly-formed oxygen dumbbells along migration path (bond switching). Similar mechanism was suggested earlier for a diffusion of interstitial oxygen atom in MgO crystal.[15] Influence of a Frenkel partner on this process is rather weak, thus, presence of remote V_O vacancy can be ignored when simulating trajectory of O_i migration in crystal and we consider further on the supercell with an additional O atom.

3.2. Migration paths of O_i atom and corresponding energy curves

Fig. 1 shows four types of O_i migration paths (I-IV) towards the nearest O_{reg} atoms relatively to a fixed dumbbell, which differ by lattice surroundings. Trajectories I and II begin and end within the same oxygen (0001) layer in α-Al_2O_3 lattice while trajectories III and IV pass between the two nearest (0001) layers. Initial lengths of the migration jumps change in the following sequence: $d_I < d_{III} < d_{II} < d_{IV}$. Fig. 2 presents the energy variation depending on path configuration for O_i:

$$O_{reg}^{initial\ dumbbell} \Rightarrow O_i \Rightarrow O_{reg}^{final\ dumbbell} \quad (4)$$

Final dumbbell configuration within the chosen migration interval is limited by the shortest distance between interstitial oxygen atom and the final O_{reg} position, corresponding to the equilibrium interatomic distance within a dumbbell, *i.e.*, 1.4 Å (Table 1). All four O_i migration paths imaged in Fig. 2 pass through the energy barriers (or transition states along the paths), which are optimized within the procedure of the distinguished reaction coordinate technique mentioned in Subsection 2.1. These barriers have been estimated to lie in the range of 1.3-1.8 eV, depending on four migration path trajectories. The highest barrier (~1.8 eV) is achieved along migration path II, the lowest barrier for 3D migration includes path III and requires the activation energy of 1.3 eV.

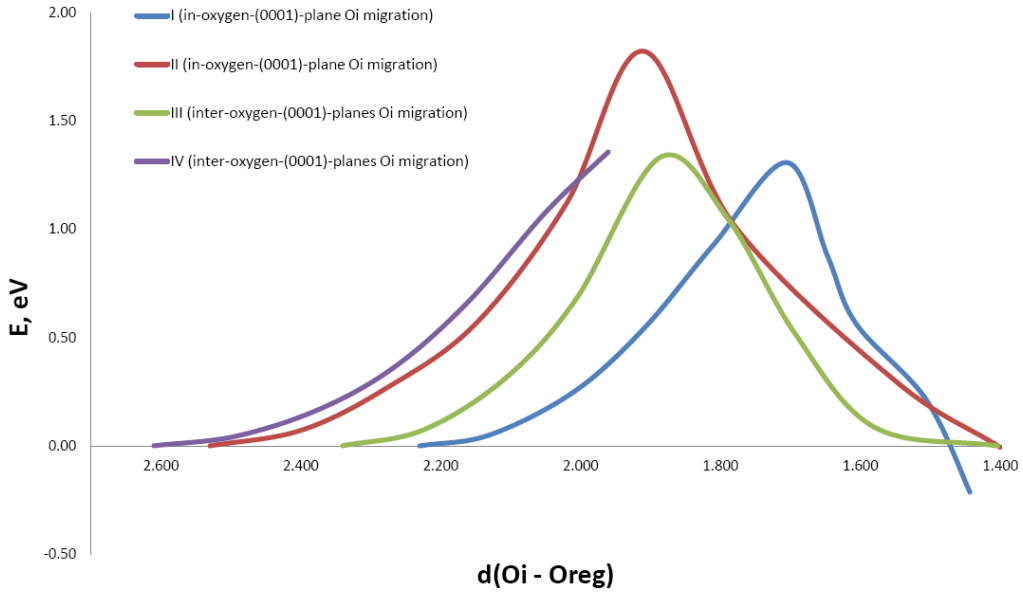

Figure 2. The energy curves for four migration paths I, II, III and IV of interstitial O_i atom in corundum (Fig. 1) and estimated energy barriers (transition states). Details of optimization procedure applied along each trajectory are explained in Subsection 3.2.

3.3. Transformation of corundum structure around trajectory of O_i migration path I

To analyze in detail structural relaxation in corundum crystal along trajectories of interstitial oxygen atom migration, we consider as example the path I (Fig. 1). (Obviously, other trajectories can be described in a similar way.) Fig. 3 shows structural changes around corresponding migration path in the two projection views: a) and b). In order to estimate parameters of structural relaxation of O and Al atoms in the three nearest coordination spheres around O_i interstitial as well as the electronic charges induced on neighboring atoms, we have selected the corresponding polyatomic fragments inside supercell (shown as shaded areas in Fig. 3). Detailed configurations of atoms within the selected areas of optimized corundum supercell and their designations are shown in Fig. 4, while their structural relaxation and charges induced by O_i are presented in Table 2. Atoms of third coordination sphere are changed along migration paths, this is why Table 2 contains a few empty cells.

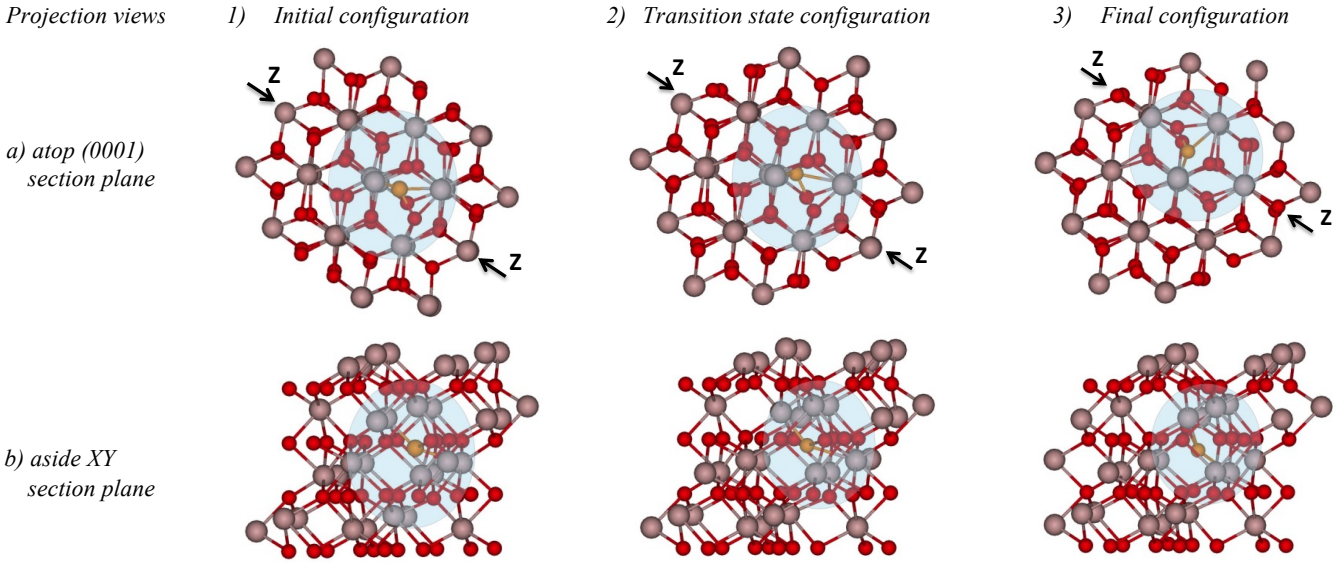

Figure 3. Structural transformation of initial (1), transition state (2) and final (3) configurations of α-Al_2O_3 2×2×1 supercell along O_i migration path I (atop and aside views). Shaded light-blue areas contain three coordination atomic spheres around interstitial oxygen atom (Fig. 4). Z-Z arrows show traces of section planes used for construction of electron density plots shown in Fig. 5. Other details are given in caption of Fig. 1.

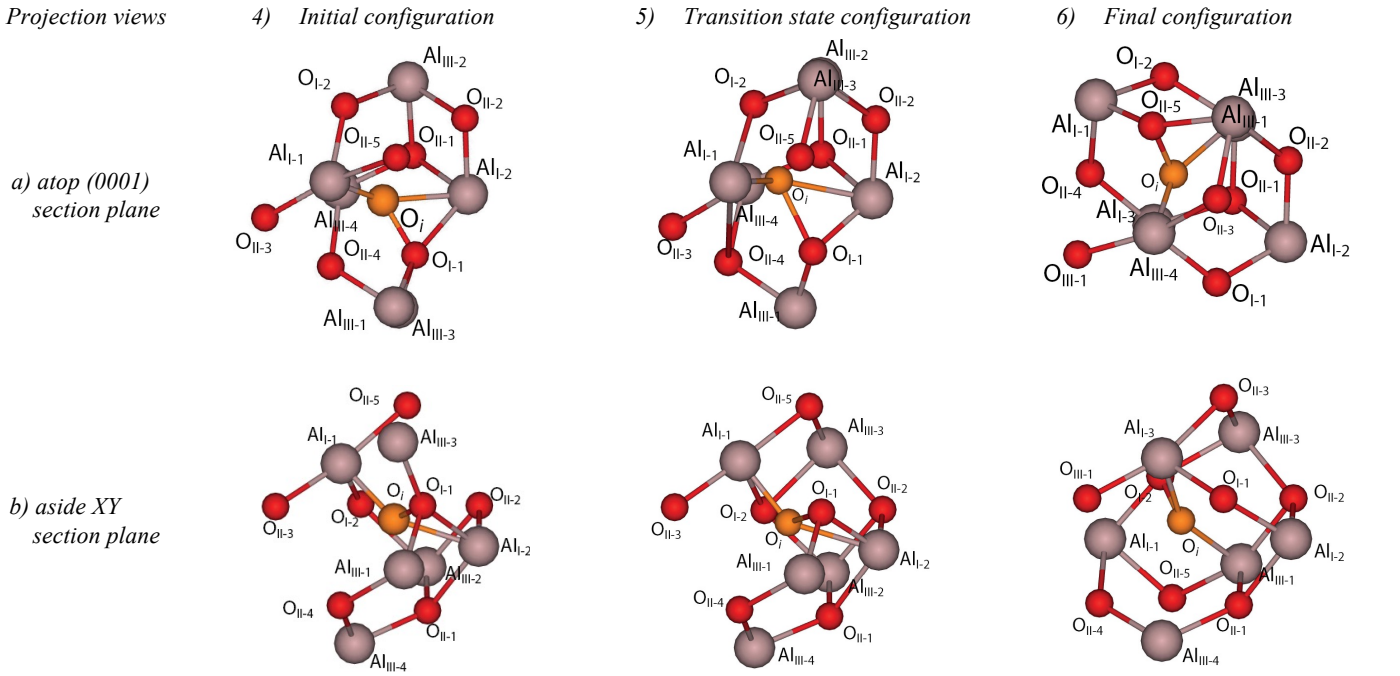

Figure 4. Structural transformation of three coordination atomic spheres around oxygen interstitial for initial (1), transition state (2) and final (3) configurations inside α-Al_2O_3 lattice along O_i migration path I (atop and aside views, analogously to Fig. 3). Enumeration of surrounding atoms is used in Table 2 for description of their relaxation and induced charges. Other details are given in caption of Fig. 1.

Conditional borders of coordination atomic spheres around O_i (Table 2) have been fixed as $1.4 < d_{O_i\text{-}X_j} < 2.3$ Å and $2.6 < d_{O_i\text{-}X_k} < 2.9$ Å, where X_j and X_k designate atoms in the corresponding spheres. Noticeable atomic relaxations and changes of electronic charges have been observed in the first coordination spheres only, except for transition state configuration, while the largest electronic charge transfer towards O_i atom occurs within dumbbell area (0.39 and 0.4 *e* in initial and final configurations, respectively, as presented in Table 2). On the other hand, O_{reg} atoms in dumbbells partially share electronic density with the nearest Al neighbors, this is why $q_{O_{reg}} > q_{Oi}$ (Table 1).

Table 2. Structural transformation of three coordination atomic spheres around oxygen interstitial and charges induced on atoms of initial, transition and final configurations inside corundum 2×2×1 supercell along O_i migration path I.

Atoms	Initial	$\|\Delta r\|$,[a] Å	Δq,[b] *e*	Transition	$\|\Delta r\|$,[a] Å	Δq,[b] *e*	Final	$\|\Delta r\|$,[a] Å	Δq,[b] *e*
1NN coordination sphere									
O_{I-1}	1.4	0.54	0.39	1.68	0.42	0.19	2.24	0.16	0
Al_{I-1}	1.74	0.28	-0.02	1.69	0.32	-0.04	1.85	0.1	0.03
Al_{I-2}	1.94	0.12	0.03	2.08	0.07	0.03	1.93	0.13	0.02
O_{I-2}	2.23	0.19	0.01	1.71	0.08	0.1	1.44	0.73	0.4
Al_{I-3}							2.26	0.16	0.03
2NN coordination sphere									
O_{II-1}	2.34	0.2	0.01	2.29	0.22	0.01	2.47	0.09	0
O_{II-2}	2.53	0.06	0.01	2.42	0.07	0.01	2.44	0.06	0.01
O_{II-3}	2.61	0.07	0.01	2.57	0.11	0.01	2.64	0.01	0
O_{II-4}	2.61	0.05	0	2.77	0.04	0	2.62	0.03	0
O_{II-5}	2.66	0.06	0	2.59	0.08	0	2.47	0.11	0.01
3NN coordination sphere									
Al_{III-1}	2.61	0.15	-0.01	2.93	0.05	0.03	2.75	0.05	0.01
Al_{III-2}	2.83	0.05	0.01	2.56	0.11	-0.02			
Al_{III-3}	2.87	0.11	-0.01	2.78	0.08	0.01	2.54	0.11	0.02
Al_{III-4}	2.87	0.04	0.02	2.82	0.05	-0.02	2.8	0.06	0.02
O_{III-1}							2.81	0.07	0

[a]structural relaxation of atoms inside three nearest coordination spheres induced by O_i atom;
[b]electronic charges on atoms inside three nearest coordination spheres induced by O_i atom.

3.4. Electron density redistribution around Oi atoms

According to the results of our previous study,8 interstitial oxygen atom, kicked off from a regular lattice site under irradiation, can be initially displaced into oxygen octahedron (formed by six nearest neighboring O_{reg} atoms positioned in the two adjacent (0001) planes of α-Al_2O_3 lattice) and is practically a neutral atom. When moving then towards O_{reg} atom, in order to form energetically the most stable oxygen dumbbell, O_i atom attracts additionally ~0.5 *e*, close to the effective charge of the neighboring oxygen, ~0.6 *e* (Table 1). As a result, the dumbbell charge -1.1 e is close to that in a regular corundum (-1 *e*). The electron density plots imaged in Figs. 5.1 and 5.3 clearly show that both dumbbell configurations O_{I-1}+O_i and O_i+O_{I-2} can be

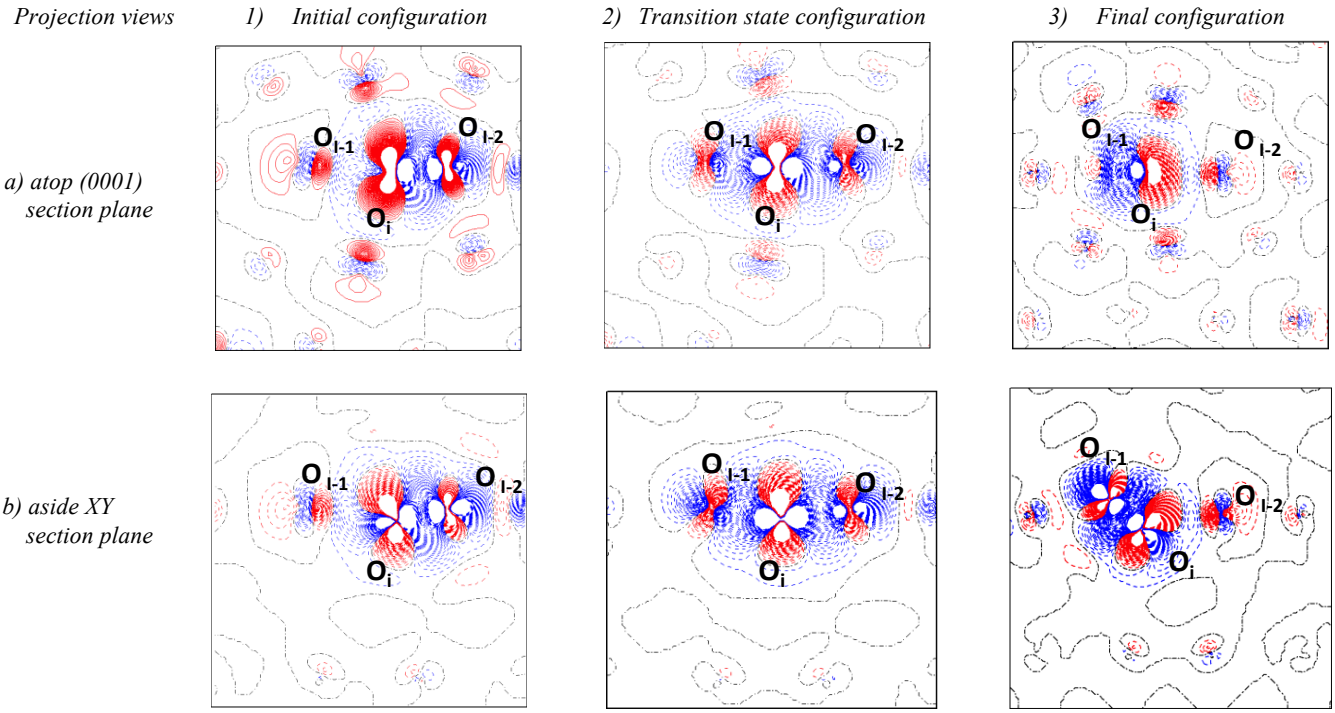

Figure 5. 2D difference electron density plots ρ(**r**) (the total electron densities in the defective corundum minus the sum of these densities in the isolated oxygen atom and the perfect α-Al_2O_3) projected onto the section Z-Z planes shown in Fig. 3. These planes cross interstitial oxygen atom as well as O_{reg} atoms (completely or partially) forming initial, transition and final O_{reg}+O_i+O_{reg} configurations. Dash-dot (black online) isolines correspond to the zero level. Solid (red) and dashed (blue) isolines describe positive and negative values of the difference in electron density, respectively. Iso-density curves are drawn from 0.05 to +0.05 *e* Å^{-3} with an increment of 0.0005 *e* Å^{-3}.

described as quasi-molecular, where both O_{reg} atoms transfer ~0.4 *e* towards regular interstitial atom (the latter dumbbell is found to be more charge-polarized as compared to the former). Remaining 0.1 *e* is transferred towards O_i from the next-nearest Al and O atoms which confirm results given in Table 1. As to the transition state O_{reg}+O_i+O_{reg} configuration, charge distribution here is more homogeneous (~0.2 and 0.1 *e* are transferred towards O_i from initial and final O_{I-1} and O_{I-2} atoms, respectively, Fig. 4). In the final dumbbell configuration, O_{I-2} atom relaxes considerably which is accompanied by asymmetry in the migration energy profile along a trajectory of O_i atom migration.

4. Conclusions

We have presented results on large-scale *ab initio* calculations on defective corundum with radiation-induced interstitial oxygen atoms kicked off from regular lattice sites. Using larger supercells, we have confirmed our recent results,[14] that migration of interstitial O_i atoms leads to the formation of dumbbells with regular oxygen atoms (O_{reg}-O_i). It has been proved that optimized configuration of fixed dumbbell is a more preferable alternative to recombination of O_i atom with V_O vacancy.

Further migration of O_i atoms can be described as dumbbell migration along different trajectories (*i.e.*, interstitial oxygen atom moves from one O_{reg} atom towards one of next-neighboring O_{reg} atoms). This result qualitatively confirms analogous conclusion drawn after theoretical simulations on impurity oxygen atom diffusion along different trajectories in MgO bulk.[15] In order to estimate O_i migration barriers (transition states), we have used the distinguished reaction coordinate technique as implemented in *CRYSTAL14* code.[24] These barriers have been found to be in the energy interval of 1.3-1.8 eV depending on migration path trajectories.

We have also estimated structural relaxations around the interstitial atom trajectories and distributions of the electron charges inside three coordination spheres around migrating O_i. atom. If interstitial oxygen is incorporated inside octahedron, formed by six nearest neighboring O_{reg} atoms positioned in the two adjacent (0001) planes of α-Al_2O_3 lattice, it is practically neutral. When moving towards O_{reg} atom, in order to form energetically most stable oxygen dumbbell, O_i atom accepts ~0.5 *e* while the effective charge of the neighboring oxygen is ~0.6 *e*, *i.e.*, O_{reg}+O_i configurations can be described as quasi-molecular radical (with interatomic distance 1.40 Å and effective charge -1.1 *e*). This is similar to the superoxide ion O_2^- well known in radiation chemistry, its bond length was found to be 1.33 Å.[3]

In our further studies, we plan to perform large-scale ab initio simulations on anion dumbbell formation in corundum the case of generation of radiation-induced O^+ ions. For this purpose, we develop cluster models of charged α-Al_2O_3 crystal for further study of oxygen ion migration.

Acknowledgments

This work has been carried out within the framework of the EUROfusion Consortium and has received funding from the European Union's Horizon 2020 research and innovation programme under grant agreement number 633053. The views and opinions expressed herein do not necessarily reflect those of the European Commission. Authors thank R Vila, A. Luchshik, and A I Popov for fruitful discussions.

References

1. *Science of Alumina*, special issue of *J. Amer. Cer. Soc.* **77** (10) (1994).

2. R.H. French, H. Müllejans, and D.J. Jones, Optical properties of aluminum oxide: Determined from vacuum ultraviolet and electron energy-loss spectroscopies. *J. Am. Ceram. Soc.* **81**, 2549–2557 (2005).

3. F. Mota, C.J. Ortiz, R. Vila, N. Casal, A. Garcia, and A. Ibarra. Calculation of damage function of Al_2O_3 in irradiation facilities for fusion reactor applications. *J. Nucl. Mater.* **442**, Suppl. 1, S699-S704 (2013).

4. A. Serikov, L. Bertalot, M.Clough, U. Fischer, and A. Suarez, Neutronics analysis for ITER cable looms. *Fusion Eng. and Design*, in press (2015).

5. P.W.M. Jacobs and E.A. Kotomin, Modeling of point defects in corundum crystals. *J. Am. Ceram. Soc.* **77**, 2505–2508 (1994).

6. B.D. Evans, A review of the optical properties of anion lattice vacancies, and electrical conduction in α-Al_2O_3: Their relation to radiation-induced electrical degradation. *J. Nucl. Mater.* **219**, 202–223 (1995).

7. E.A Kotomin, A.I. Popov, and A. Stashans, Computer modeling of radiation damage in cation sublattice of corundum. *Phys. Status Sol. B* **207**, 69-73 (1998).

8. E.A. Kotomin and A.I. Popov, Radiation-induced point defects in simple oxides (review article). *Nucl. Instr. Meth. B* **141,** 1-15 (1998).

9. R.S. Averback, P. Ehrhart, A.I. Popov, and A. von Sambeek, Defects in ion implanted and electron irradiated MgO and Al_2O_3. *Rad. Eff. Def. Solids* **136** 169-173 (1995).

10. E.A. Kotomin, A.I. Popov, and A. Stashans, A novel model for F^+ to F photoconversion in corundum crystals. *J. Phys.: Cond. Mat.*, **6**, L 569-L573 (1994).

11. A. Lushchik, Ch. Lushchik, K. Schwartz, E. Vasil'chenko, T. Karner, I. Kudryavtseva, V. Isakhanyan, and A. Shugai, Stabilization and annealing of interstitials formed by radiation in binary metal oxides and fluorides. *Nucl. Instr. Meth. B* **266**, 2868-2871 (2008).

12. A. Lushchik, Ch. Lushchik, K. Schwartz, F. Savikhin, E. Shablonin, A. Shugai, and E. Vasil'chenko, Creation and clustering of Frenkel defects at high density of electronic excitations in wide-gap materials. *Nucl. Instr. Meth. B* **277**, 40–44 (2012).

13. Y. Lei, Yu Gong, Zh. Duan, G. Wang, Density functional calculation of activation energies for lattice and grain boundary diffusion in alumina. *Phys. Rev. B* **87**, 214105 (2013).

14. A. Platonenko, S. Piskunov, Yu.F. Zhukovskii, and E.A. Kotomin, *Ab initio* simulations on Frenkel pairs of radiation defects in corundum. *IOP Conf. Ser. Mater. Sci. Eng.* **77**, 012001 (1-5) (2015).

15. T. Brudevoll, E.A. Kotomin, and N.E. Christensen, Interstitial oxygen atom diffusion in MgO. *Phys. Rev. B* **53,** 7731–7735 (1996).

16. A.L. Shluger, V.E. Puchin, T. Suzuki, K. Tanimura, and N. Itoh, N. Optical transitions of the *H* centers in alkali halides. *Phys. Rev. B* **52** 4017- 4018 (1995).

17. K. Matsunaga, T. Tanaka, T. Yamamoto, and Y. Ikuhara, First principles calculations of intrinsic defects in Al_2O_3. *Phys. Rev. B* **68**, 085110 (1–9) (2003).

18. J. Maeda and T. Okada, Theoretical study of optical transitions of *H* centers in potassium halides. *J. Lum.*, **87**, 564-567 (2000).

19. E.A. Kotomin, V.E. Puchin, and P.W.M. Jacobs, A theoretical study of *H* center migration in alkali halide crystals KCl and NaCl. *Philos. Mag. A* **68,** 1359–1367 (1993).

20. M.T.E. Halliday, W.P. Hess, and A.L. Shluger, Structure and properties of electronic and hole centers in CsBr from theoretical calculations. *J. Phys.: Cond. Matt.*, **27**, 245501 (2015).

21. L. Yue, R. Jia, H. Shi, X. He, and R.I. Eglitis, First-principles calculations for the *H* center in SrF_2 crystals. *J. Phys. Chem. A* **114**, 8444–8449 (2010).

22. H. Shi, R. Jia, and R.I. Eglitis, First-principles simulations of *H* centers in CaF_2. *Comput. Mater. Sci.* **89,** 247–256 (2014).

23. F.U. Abuova, E.A. Kotomin, V.M. Lisitsyn, A.T. Akilbekov, and S. Piskunov, *Ab initio* modeling of radiation damage in MgF_2 crystals. *Nucl. Instr. Methods in Phys. Res. B* **326,** 314–317 (2014).

24. R. Dovesi, V.R. Saunders, C. Roetti, R. Orlando, C.M. Zicovich-Wilson, F. Pascale, B. Civalleri, K. Doll, N.M. Harrison, I.J. Bush, Ph. D'Arco, M.Llunell, M. Causá M, and Y. Noël, *CRYSTAL14 User's Manual* (University of Torino, 2014).

25. J. Baima, A. Erba, M. Rérat, R. Orlando , and R. Dovesi, Beryllium oxide nanotubes and their connection to the flat monolayer. *J. Phys. Chem. C* **117**, 12864–12872 (2013).

26. M. Causá, R. Dovesi, and C. Roetti, Pseudopotential Hartree-Fock study of seventeen III-V and IV-IV semiconductors. *Phys Rev B* **43**, 11937- 11943 (1991).

27. A.D. Becke, Density-functional thermochemistry. *iii*. The role of exact exchange. *J. Chem. Phys.* **98**, 5648–5652 (1993).

28. H.J. Monkhorst and J.D. Pack, Special points for Brillouin-zone integrations. *Phys. Rev. B* **13**, 5188-5192 (1976).

29. R.S. Mulliken, Electronic population analysis on LCAO-MO molecular wave functions. I. *J. Chem. Phys.* **23**, 1833-1840 (1955).

30. C.M. Zicovich-Wilson, M.L. San-Román, and A. Ramírez-Solís, Mechanism of F^- elimination from zeolitic D4R units: A periodic B3LYP study on the octadecasil zeolite. *J. Phys. Chem. C* **114**, 2989-2995 (2010).

31. *CRC Handbook of Chemistry and Physics* (74th Ed., edited by D.R. Lide, CRC Press, Boca-Raton, FL, 1993).

32. H. Kung, *Transition Metal oxides: Surface Chemistry and Catalysis*, (Elsevier, NY, 1989).